

Article

# Control Strategy of an Impulse Turbine for an Oscillating Water Column-Wave Energy Converter in Time-Domain Using Lyapunov Stability Method

Seung Kwan Song and Jin Bae Park \*

Department of Electrical and Electronic Engineering, Yonsei University, 50 Yonsei-ro, Seodaemun-gu, Seoul 03722, Korea; nomadnosad@gmail.com

\* Correspondence: jbpark@yonsei.ac.kr; Tel.: +82-2-2123-2773

Academic Editors: Frede Blaabjerg and Yongheng Yang

Received: 26 July 2016; Accepted: 23 September 2016; Published: 2 October 2016

**Abstract:** We present two control strategies for an oscillating water column-wave energy converter (OWC-WEC) in the time domain. We consider a fixed OWC-WEC on the open sea with an impulse turbine module. This system mainly consists of a chamber, turbine and electric generator. For the time domain analysis, all of the conversion stages considering mutualities among them should be analyzed based on the Newtonian mechanics. According to the analysis of Newtonian mechanics, the hydrodynamics of wave energy absorption in the chamber and the turbine aerodynamic performance are directly coupled and share the internal air pressure term via the incompressible air assumption. The turbine aerodynamics and the dynamics of the electric generator are connected by torque load through the rotor shaft, which depends on an electric terminal load that acts as a control input. The proposed control strategies are an instant maximum turbine efficiency tracking control and a constant angular velocity of the turbine rotor control methods. Both are derived by Lyapunov stability analysis. Numerical simulations are carried out under irregular waves with various heights and periods in the time domain, and the results with the controllers are analyzed. We then compare these results with simulations carried out in the absence of the control strategy in order to prove the performance of the controllers.

**Keywords:** wave energy converter; oscillating water column; turbine control strategy

## 1. Introduction

Technologies that efficiently harness the power of ocean waves are now emerging, setting the stage for ocean waves to become a new major renewable energy source [1,2]. These technologies have great potential and can be used in tandem, with other renewable energy sources, such as wind and solar, to cater to peak energy demands. Various groups have successfully developed several types of wave energy converters (WECs) at the lab scale, and several models have now been installed in the oceans for commercial testing [3,4].

In order to permit analytic development, the optimization procedure and control strategy should be considered. The optimization is to determine the parameters of the model geometry and the physical component under constraints [5–9]. In addition, the control strategy for how to tune the power take-off (PTO) needs to be determined to maximize the consistency of the extracted power in response to the wave variation in height and frequency due to changes in the ocean environment condition from hourly to annually. Initial studies employing the control strategy for WECs revealed that impedance matching provides the theoretical maximum useful energy for a body oscillating in one mode [10–12]. However, this strategy requires a preemptive knowledge of the body's velocity and/or excitation force of the waves, making it impossible to implement in practice. Furthermore,

it requires an ideal (or close to ideal) PTO, which must be able to readily switch between the functional roles of a generator and actuator with high converting efficiency. This in turn would allow control over the sign and magnitude of the hydrodynamic stiffness and the damping coefficient [13,14].

One of the control techniques that requires a relatively low level of WEC's hydrodynamic information with a reactive energy flow is latching control. This method was first applied to a single heaving buoy [15] and was later also applied to two-body systems [16,17]. This technique only requires the stopper and not the actuator function of the PTO. However, it does require information regarding peak moments of upcoming ocean waves.

Oscillating water column (OWC)-WECs have also been widely studied. OWC-WEC, which is simpler in terms of configuration, was first designed for use in marine navigation [18–20]. Later, OWC-WEC research mainly focused on fixed systems along the coast [21–23] and floating systems on the open sea [7,8,24–26].

OWC-WECs essentially consist of a capture chamber, a turbine and an electrical generator. Compared to the moving body types, they have a relatively simple mechanical structure, since there is no mechanical elements, such as a hinge, shaft or linear guide. Incident waves cause the inner water surface level of the capture chamber to oscillate. The reciprocating air flow resulting from the pressure fluctuations in the chamber drives the turbine. The electric generator connected to a turbine rotor then converts the rotational kinetic energy into electricity. The direction and speed of the air flow supplied to the turbine are frequently changed via movement of the waves. As such, an impulse turbine [27,28] or Wells turbine [29], which rotates in one direction regardless of the direction of air flow, is commonly fitted to circumvent the air to the electricity energy conversion problem in OWC-WEC systems.

Efforts have been made to improve the efficiency of OWC-WECs by using a control strategy. However, as an impedance matching control, the PTO module itself acts as an ideal actuator. In OWC-WEC, the self-rectifying air turbine, which functions as the PTO module is unable to work as an actuator. As a result, in order for the impedance matching control to be applied to OWC-WEC, a highly-efficient compressor must be introduced to make its application impractical [30–32]. Jefferys et al. [33] presented a latching control strategy for OWC-WEC, which considers air compressibility. Hoskin et al. [34] were the first to apply a phase controller to the OWC-WEC by making the damping coefficient proportional to the device's velocity. These studies all aimed at developing strategies to maximize the conversion efficiencies in the chamber stage (first stage). However, since OWC's overall efficiency is also influenced by the turbine stage (second stage), control strategies to ensure the turbine's efficiency would also be of benefit to the system. The power of air flow induced by the water column oscillation is transferred to the turbine, and the resultant turbine rotation in turn affects the motion of the water column. Thus, control strategies that consider the entire system including the turbine stage were introduced in [6,35–39].

In [6,35,36], the frequency domain analysis is introduced to calculate a large number of simulations that consider various ocean states. It is assumed, however, that the turbine rotational speed remains constant, thereby resulting in a large rotational inertia. However, under these conditions, the turbine cannot respond in a low level of sea energy state. In addition, since this analysis is done in the frequency domain, the moment controller strategies in the time domain were not allowed.

In [37–39], control strategies to avoid stalling were introduced, since when using the Wells turbine, stalling drastically reduces the efficiency. These analyses were based on the Newtonian mechanics, so performed in the time domain, and analyzing the effect of the control strategy impact on the turbine stage was carried out. Because the effect of turbine stage on the chamber stage is not taken into account, the effect of control strategy impact on the overall system efficiency was not analyzed.

In summary on the previous studies on the optimization and control theory of OWC-WECs including turbine aerodynamics, it can be mainly categorized as the frequency domain analysis and time domain analysis; they have their own pros and cons. The analysis of the frequency domain takes into account the compressibility of air and provides the direct substitution of the wave spectrum into the analysis, but the turbine aerodynamics based on the Newtonian mechanics is impossible,

which brings the assumption of the turbine's constant angular speed [6,35,36]. Otherwise, the time domain analysis is able to address the angular acceleration of the turbine rotor since it is based on the Newtonian mechanics [27,28,37–39]. Therefore, it is not necessary to assume the constant angular speed of the turbine rotor.

We choose the time domain analysis in order to develop a real-time control law for OWEC-WECs considering turbine aerodynamics. We investigate a system that combines the hydrodynamics of the chamber, the aerodynamics of the impulse turbine and the modeling of an ideal DC generator, as shown in Figure 1. Unlike the analysis in the frequency domain, analysis in the time domain is based on the Newtonian mechanics, and it considers the angular acceleration of the turbine rotor. In the turbine aerodynamics, the pressure on the turbine, induced torque from the electric generator and turbine rotor inertia are taken into account and determine the angular acceleration of the turbine rotor in real time. Accordingly, it requires no assumption of constant rotor angular speed for the frequency domain, and rotor inertia acts as an important variable.

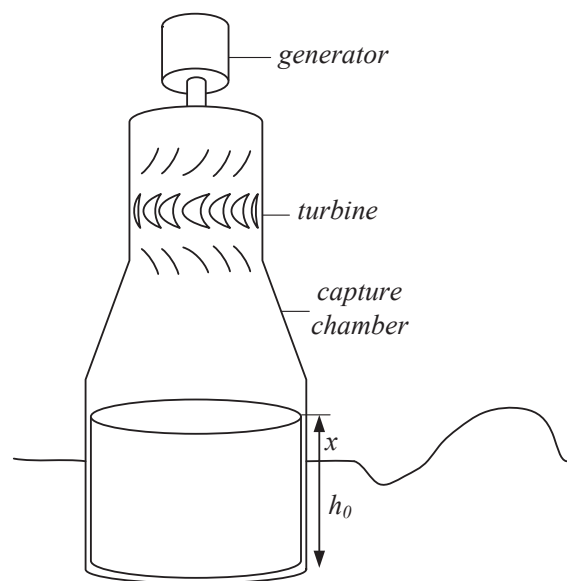


**Figure 1.** A model of the oscillating water column (OWC).

We put forth two strategies for the controller. First is a strategy that maximizes the turbine's instant efficiency. The second strategy attempts to maintain the rotational speed at a constant rate. These two methods are differentiated by the definition of the reference angular velocity and can be induced by the Lyapunov stability theory [40–43]. The aforementioned controllers can be implemented by a load control that is attached to the ideal DC generator. We investigate the performance of the controllers through simulation in the time domain under irregular waves. Furthermore, we run simulations in various wave periods and heights and compare and analyze the performance of the strategies with and without the controller.

## 2. Model Description

We assume the OWC-WEC fixed in a position relative to the sea bed as illustrated in Figure 1. As waves pass by, water inside the chamber oscillates, causing the air inside the chamber to compress and expand. This results in a pressure difference between the atmosphere and internal chamber, which in turn causes the impulse turbine to rotate. In this process, it is assumed that the incompressible internal air yields a direct coupling of the chamber's hydrodynamics and the turbine dynamics. This assumption has the limitation that the spring-like effect of the air is ignored, and air flows in the exhausting and inhaling process are equivalent. However, the turbine rotor speed becomes the time-varying variable. A main objective of this paper is to analyze the effect of the turbine controller

on the overall performance of a three-stage system comprising a capture chamber (first stage), impulse turbine (second stage) and electric generator (third stage). Hence, we have simplified the configuration of each stage as described in the following subsections.

### 2.1. Capture Chamber

The capture chamber is a vertical hollow cylindrical structure with openings at both ends. It is fixed in position and partly immersed in the sea. The impulse turbine is located at the upper end, and the lower end is exposed to the water. Air flowing through the turbine provides a resistor due to the pressure difference. Including this force, the dynamic equation of the water column inside can be expressed as follows, where  $x$  represents the level of the internal water column along the vertical [27,28,38]:

$$(M + \mu(\infty)) \ddot{x} + k_h x + F_r(t) + \Delta p_c \cdot a_c = F_e(t). \tag{1}$$

Here:

$$\begin{aligned} M &= \rho_w a_c (h_0 + x), \\ \Delta p_c &= \Delta p_t \operatorname{sgn}(\dot{x}(t)) + \frac{1}{2} \rho_a \left\{ \left( \frac{a_c}{a_t} \right)^2 - 1 \right\} \dot{x}^2, \\ F_e(t) &= \int_{-\infty}^{\infty} \lambda(\tau) f_e(t - \tau) d\tau, \\ F_r(t) &= \int_0^t f_r(t - \tau) \dot{x}(\tau) d\tau. \end{aligned}$$

Among them,  $F_r$  can be expressed as the following fourth order state linear equation given as:

$$\dot{z} = \mathbf{A}z + \mathbf{B}\dot{x}, \tag{2}$$

$$F_r(t) = \mathbf{C}z, \tag{3}$$

where  $z(t) \in \mathbb{R}^{4 \times 1}$  is a fictitious radiation state vector, while  $\mathbf{A} \in \mathbb{R}^{4 \times 4}$ ,  $\mathbf{B} \in \mathbb{R}^{4 \times 1}$  and  $\mathbf{C} \in \mathbb{R}^{1 \times 4}$  are the radiation model state and input and output matrices, respectively [44]. This subsystem has the velocity as the input and the radiation force as the output.

### 2.2. Impulse Turbine

The dynamics of the impulse turbine typically assumes steady uni-directional air flow, even though the actual characteristics are that of bi-directional motion with fluctuating speed. Hence, we assume this process as a quasi-steady state; doing so will provide the applicability of the steady flow characteristics of the turbine into the second stage. The dynamics is presented as follows [27]:

$$\Delta p_t = C_a \cdot \beta \cdot \frac{1}{a_t} \cdot V_x^2 \left[ 1 + \frac{1}{\phi^2} \right], \tag{4}$$

$$\tau_t = C_t \cdot \beta \cdot r_t \cdot V_x^2 \left[ 1 + \frac{1}{\phi^2} \right], \tag{5}$$

$$\eta_t = \frac{P_t}{P_{pne}} = \frac{\tau_t \Omega}{\Delta p_t \cdot Q} = \frac{C_t}{C_a \cdot \phi}, \tag{6}$$

with:

$$\phi = \frac{V_x}{r_t \Omega}, \tag{7}$$

$$\beta = \frac{\rho_a b_t l_t n_t}{2}, \tag{8}$$

$$Q = a_t V_x = a_c |\dot{x}|. \tag{9}$$

It is emphasized that the inside air is incompressible; therefore, flow rate  $Q$  can be proportional to  $V_x$  and  $|\dot{x}|$ .  $C_a$ ,  $C_t$  and  $\eta_t$  are functions of  $\phi$  and should be numerically modeled in order to carry out the simulation. Hence,  $C_a$  and  $C_t$  are assumed to be numerical equations of  $\phi$  as follows [45]:

$$C_a = -0.02358 + 3.4556\phi + 3.9422\phi^2 - 11.1530\phi^3 + 10.4871\phi^4 - 5.0828\phi^5 + 1.2673\phi^6 - 0.1285\phi^7. \tag{10}$$

$$C_t = -0.042480 - 0.5936\phi + 2.9063\phi^2 + 0.1824\phi^3 - 2.6953\phi^4 + 1.9518\phi^5 - 0.8781\phi^6 + 0.06377\phi^7. \tag{11}$$

$\phi$  is assumed to be bounded within  $0.5 < \phi < 2.5$ . In Figure 2, it can be seen that  $C_a$  continuously increases from the origin, but  $C_t$  starts from a negative value with small  $\phi$  and gradually increases.

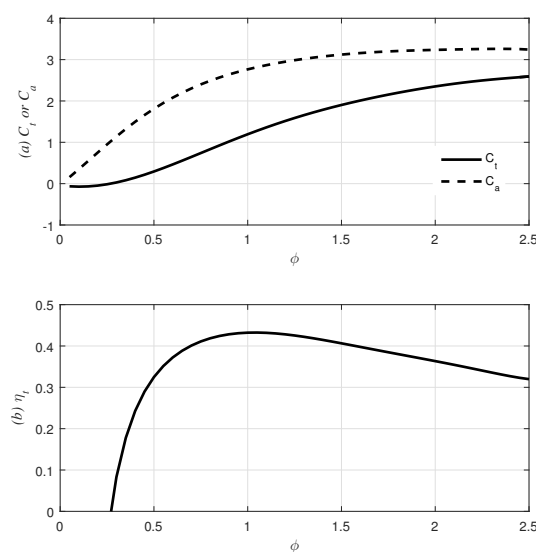


**Figure 2.** Turbine characteristics: (a) input and torque coefficients; (b) turbine efficiency.

The governing equation for the turbine motion is:

$$J\dot{\Omega} = \tau_t - \tau_g. \tag{12}$$

The left-hand side represents the inertia torque. The right-hand side is the sum of turbine output torque and load torque induced from an electric generator.

### 2.3. Electric Generator

In general, the PTO module applied to the wave energy converter is assumed to be a linear damper, which provides a damping force proportional to the speed. An ideal DC generator corresponds to the ideal linear damper. Thus, it provides the following characteristics [46]:

$$\tau_g = K_g I_a, \tag{13}$$

$$E_g = K_g \Omega = (R_a + R_e) I_a. \tag{14}$$

From (13) and (14), the following equation can be established.

$$\tau_g = b_g \Omega, \tag{15}$$

where:

$$b_g = \frac{K_g^2}{R_e + R_a}. \tag{16}$$

Since the maximum efficiency of the typical electric generator is mainly decided by the volume, size and materials of the generator, it is a much more practical process and is not appropriate when considering the basic modeling level for the initial control strategy. In general, matching the relatively larger terminal load provides a higher efficiency, but also provides a lower generator torque to the turbine and a lower power output.

In this paper, the analysis of entire system performance via the terminal load control through the turbine and chamber stage is mainly the focus. Hence, it is assumed that the internal load is relatively smaller than the external terminal load, and this denotes the ideal DC generator applied on the system. When external load  $R_e$  is large relative to the internal load  $R_a$ , the loss on the internal load can be ignored, and the efficiency of the electric generator can approach one, while ignoring mechanical losses. Consequently, power sent to the generator  $P_g$  is equivalent to  $P_t$ . Therefore, the instantaneous generated power can be written as:

$$P_t \simeq P_g = b_g \Omega^2. \tag{17}$$

Hereafter, the terminal power extraction will be regarded as  $P_t$ .

### 3. Controller Design and Stability Analysis

#### 3.1. Control Design Objective

A majority of research on control strategies for WECs has focused on the first stage of the system [17,34,47]. Here, we will only focus on that of the turbine stage. Previous studies have dealt with control strategies of an OWC-WEC with the turbine module [9,35,36]. These papers assume that blade inertia is large enough for the turbine angular speed to remain constant. However, these studies do not cover the effects of electric generator load on the turbine system in the time domain.

In the previous section, our turbine modeling provides the input states ( $\Delta p_t$  and  $b_g$ ) and the outputs ( $\Omega$  and  $V_x$  (or  $\dot{x}$ )). Here, we emphasize that  $b_g$  is the only controllable parameter. Thus, this study presents control strategies for the impulse turbine where the control input is  $b_g$ .

Two major issues arise when considering the turbine's characteristics and power quality. These issues relate to (1) the maximum turbine efficiency and (2) the constancy of the output voltage. As shown in Figure 2, the efficiency of the turbine is a function of  $\phi$  and has a single peak point. This optimal point will herein be referred to as  $\phi_o$ . For the first issue, it can be determined from (7) that the reference rotor angular velocity (or desired angular velocity)  $\Omega_d$  becomes a function of time varying state  $V_x$  as:

$$\Omega_d = \phi_o / r_t \cdot V_x. \tag{18}$$

Consequently, the control objective for the maximum turbine efficiency is to make  $\Omega$  track the time-varying desired angular velocity  $\Omega_d$ .

Furthermore, a constant supply of voltage is important for the quality of generated electric power. It is hugely advantageous to provide a constant voltage in terms of usability and workability while providing irregular current. Whether charging a battery directly or connecting it to the converter, electricity with a constant voltage is more utilizable than that with a constant current. Equation (14) states that the output voltage is proportional to the rotor speed. As such, generating a constant output voltage relies heavily on maintaining a constant rotor speed. Thus, for the second issue, the control objective is to make  $\Omega$  converge to the constant desired angular velocity  $\Omega_d$ .

It should be noted, however, that maximum turbine efficiency and constant output voltage cannot be simultaneously achieved. Hence, upon reaching maximum turbine efficiency, the output voltage must be swung according to  $V_x$ . Conversely, if a constant voltage output is achieved, the turbine efficiency will subsequently be sub-optimal. Nonetheless, both parameters are determined by  $\Omega$ , and

consequently, choosing  $\Omega_d$  will determine the control purpose. From this point, the former will be referred to as the i-MET (instantaneous-maximum efficiency tracking) control and the latter as the CAV (constant angular velocity) control, respectively.

### 3.2. Stability Analysis

We present the i-MET and CAV controllers using stability analysis based on Lyapunov’s theory [40–43]. We use the damping coefficient of the generator  $b_g$  as a control input. This value must be positive since it is assumed that the electric generator can only convert kinetic energy to electric energy, while the reverse process is not possible. Thus, our analysis assumes that this controller only performs with a positive  $b_g$  value. As mentioned above, both controllers share the objective of tracking  $\Omega_d$ . However,  $\Omega_d$  for the i-MET strategy is time varying, whilst  $\Omega_d$  for the CAV strategy remains constant.

Consider the dynamic equation of the system obtained from (12) and (13) as:

$$\dot{\Omega} = \frac{1}{J}\tau_t - \frac{b_g}{J}\Omega. \tag{19}$$

With tracking error  $\tilde{\Omega} = \Omega - \Omega_d$ , the control law can be designed as:

$$b_g = \frac{1}{\Omega} \left\{ k_p \tilde{\Omega} + \gamma \tanh \left( \frac{\gamma \tilde{\Omega}}{\epsilon} \right) \right\}, \tag{20}$$

where  $k_p > 0, \epsilon > 0$  and  $\gamma = J\dot{\Omega}_{max} + \tau_{t,max}$  is a switching variable with  $|\dot{\Omega}_d| < \dot{\Omega}_{max}$  and  $|\tau_t| < \tau_{t,max}$ .

In order to derive the control law, let us define the Lyapunov candidate as:

$$V = \frac{1}{2}J\tilde{\Omega}^2. \tag{21}$$

The time derivative of (21) with substituting (20) yields:

$$\begin{aligned} \dot{V} &= \tilde{\Omega} \left\{ -k_p \tilde{\Omega} - J\dot{\Omega}_d + \tau_t - \gamma \tanh \left( \frac{\gamma \tilde{\Omega}}{\epsilon} \right) \right\} \\ &\leq -k_p \tilde{\Omega}^2 + |\gamma \tilde{\Omega}| - \gamma \tilde{\Omega} \tanh \left( \frac{\gamma \tilde{\Omega}}{\epsilon} \right). \end{aligned} \tag{22}$$

Using the following the hyperbolic tangent function property ( $\zeta$ : real number):

$$0 \leq |\zeta| - \zeta \tanh \left( \frac{\zeta}{\epsilon} \right) \leq 0.2785\epsilon. \tag{23}$$

$\dot{V}$  yields:

$$\begin{aligned} \dot{V} &\leq -k_p \tilde{\Omega}^2 + 0.2785\epsilon \\ &= -\frac{2k_p}{J}V + c, \end{aligned} \tag{24}$$

where  $c = 0.2785\epsilon$ .

Multiplying (24) by  $\exp(2k_p t/J)$  and integrating over  $[0, t]$  provides:

$$0 \leq V(t) \leq V(0) \exp \left( -\frac{2k_p}{J}t \right) + \frac{J}{2k_p}c. \tag{25}$$

Therefore,  $V(0)$  disappears in  $V(t)$  as time increases and  $V(t)$  converges with a boundary of  $\frac{J}{2k_p}c$ .  $c$  is the settable variable and defined as an arbitrarily small constant. As a result, the tracking error  $\tilde{\Omega}$  becomes arbitrarily small. In the process of the stability proof for the controller,  $\Omega$  becomes  $\Omega_d$  with small margin of error.

#### 4. Simulation Results under Irregular Waves in the Time Domain

We carry out simulations of the OWC system associated with the control strategies in the time domain. For time domain calculations, a Runge–Kutta method [48] was applied for solving the above dynamics under irregular wave condition.

We obtain the hydrodynamic parameters of the first stage from ANSYS AQWA[49] using the assumption that a trapped water column is regarded as a rigid body of a cylindrical shape. In the simulation, the body has a 6-m diameter with a 5-m draft ( $h_0$ ) floating in the ocean cube that has a 500 by 500 m<sup>2</sup> surface and a 50-m water depth, and only the heave motion of the body is allowed. In order to properly calculate heave impulse response function, the frequency domain response should have a truncation frequency of 2 rad/s with a frequency spacing of 0.05 rad/s [50].

The solid lines in Figure 3 display the impulse response of excitation force  $f_e$  and radiation force  $f_r$  for calculations of  $F_e$  and  $F_r$ , respectively, and the dashed line is for the state space approximation for  $f_r$ .

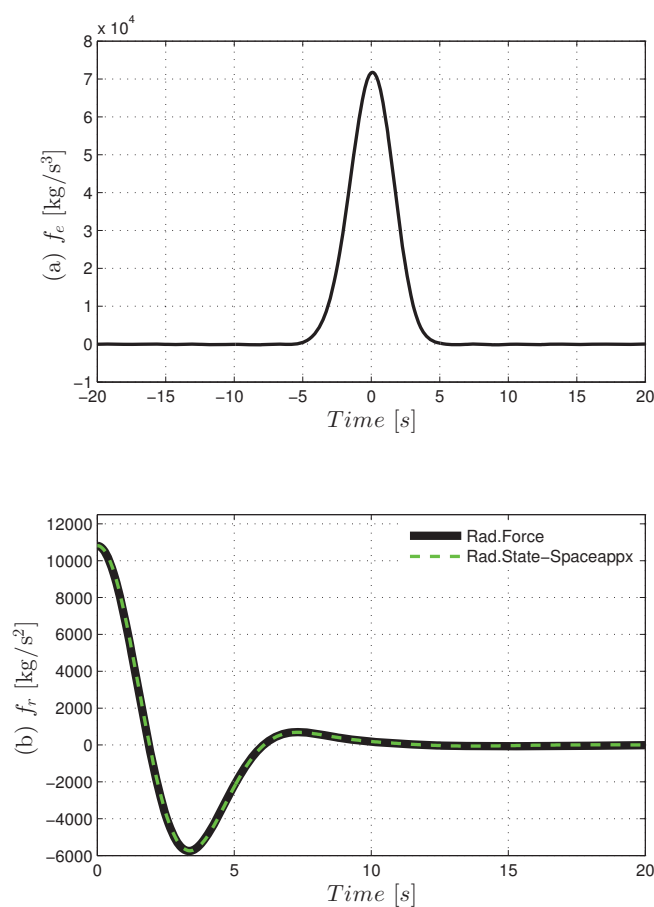


**Figure 3.** Impulse response functions: (a) excitation force; (b) radiation force and its state-space approximation.

A Pierson–Moskowitz (PM) wave model is applied to analyze the performance of the device. When a constant wind has blown for a sufficiently long time along a sufficiently long stretch of the ocean, the semi-empirical PM spectrum [51]:

$$S_{PM}(\omega) = 5\pi^4 \frac{H_s^2}{T_p^4} \frac{1}{\omega^5} \exp\left(-\frac{20\pi^4}{T_p^4 \omega^4}\right), \tag{26}$$

matches relatively well with the experimentally-obtained wave spectra, where  $H_s$  and  $T_p$  denote significant wave height and the peak wave period, respectively.

For time series calculations, the spectral distribution (26) is discretized as the sum of a large number  $N$  of regular waves as written as:

$$\lambda(t) = \sum_{n=1}^N \lambda_n \cos(\omega_n t + \theta_n). \tag{27}$$

Here,  $\omega_n = \omega_l + (n - 1)\Delta\omega$ , where  $\omega_l$  is the lowest frequency,  $\Delta\omega$  is a small frequency interval,  $n = 1, 2, \dots, N$  and the spectrum is not to contain a significant amount of energy outside the frequency range  $\omega_l \leq \omega \leq \omega_l + (N - 1)\Delta\omega$ .  $\lambda_n = \sqrt{2S_{PM}(\omega_n)\Delta\omega}$  and  $\theta_n$  are the amplitude of the wave component of order  $n$  and the initial phase randomly chosen in the interval  $(0, 2\pi)$ , respectively. A summary of the parameters and values used in calculations is given in Table 1.

**Table 1.** Parameters and values in the simulations.

Parameter	Value	Unit
$a_c$	28.26	m <sup>2</sup>
$a_t$	0.0254	m <sup>2</sup>
$b_t$	0.03	m
$h_0$	5	m
$k_h$	283.87	N/m
$l_t$	0.03	m
$n_t$	10	
$r_t$	0.135	m
$J$	1 (or 5)	kg/m <sup>2</sup>
$\mu(\infty)$	51,070	kg
$\rho_a$	1.226	kg/m <sup>3</sup>
$\rho_w$	1025	kg/m <sup>3</sup>
$\phi_0$	1.03	

We performed the simulation under various wave heights and periods, but only one condition was chosen for verification of the controller operation under irregular waves with  $H_s = 2$  m and  $T_p = 10$  s. The sampling time interval is 0.02 s.

#### 4.1. Result of the i-MET Controller

We carry out the simulation of an OWC-turbine combined system with an i-MET controller given as (20) with (18) under the PM wave condition in the time domain using a fourth order Runge–Kutta method. Between all i-MET controller’s gains  $k_p$ ,  $\gamma$  and  $\epsilon$ ,  $k_p$  had the greatest effect on the controlled result. Therefore, with fixed gains  $\gamma$  and  $\epsilon$  set at 100 and 0.01, respectively, we observe the difference in performance with varying  $k_p$  values. Figures 4 and 5 show the results of the first 30 s of the simulation, when  $k_p$  is set at 0.5 and 10, respectively. It can be observed in both graphs that  $\Omega_d$  changes consistently to follow  $\phi_0 = 1.03$  by (18) with the fluctuation of  $V_x$ . Through comparisons between both graphs, however, it can be seen that a result of  $k_p = 10$  produces a better performance than that of  $k_p = 0.5$  in terms of control purposes, since  $\Omega$  tracks  $\Omega_d$  closer and more quickly. This yields that the longer duration of the instant efficiency  $\eta_t$  is able to reach the maximum value with  $k_p = 10$ .

To improve the accuracy of our analysis, we obtained values for average power extraction from the turbine  $\bar{P}_t$ , average turbine efficiency  $\bar{\eta}_t$  and the relative root mean squared error of  $\Omega$  ( $RMSE^*(\Omega)$ ) by changing  $k_p$  to a value between 0.1 and 10 for 5000-s intervals ( $T_m$ ).  $\bar{\eta}_t$  is expressed as the ratio between the time integral value of the pneumatic power and the power extraction from the turbine.  $RMSE^*(\Omega)$  is the relative root mean squared error of the  $\Omega$  with respect to average desired angular velocity  $\bar{\Omega}_d$  for the times when the controller is functioning. These can be expressed as follows:

$$\bar{P}_t = \frac{1}{T_m} \int_0^{T_m} P_t dt = \frac{1}{T_m} \int_0^{T_m} b_g \Omega^2 dt, \tag{28}$$

$$\bar{\eta}_t = \frac{\int_0^{T_m} b_g \Omega^2 dt}{\int_0^{T_m} \Delta p_t \cdot Q dt}, \tag{29}$$

$$RMSE^*(\Omega) = \frac{1}{\bar{\Omega}_d} \sqrt{\frac{\sum_n \left\{ \int_{t_{n,i}}^{t_{n,f}} \tilde{\Omega}^2 dt \right\}}{\sum_n \left\{ t_{n,f} - t_{n,i} \right\}}}. \tag{30}$$

Here,  $t_{n,i}$  and  $t_{n,f}$  represent the beginning and the end times, respectively, of when the controller is working at the  $n$ -th order, which is equivalent to  $b_g > 0$ .

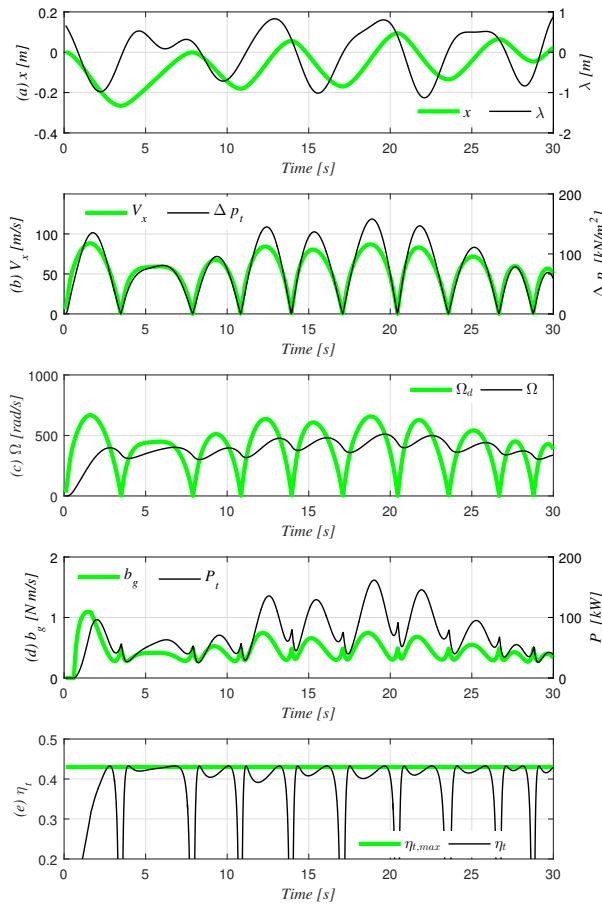


**Figure 4.** Simulation result of the first 30 s with the instantaneous-maximum efficiency tracking (i-MET) controller when  $k_p = 0.5$ : (a) wave  $\lambda$  and water column positions  $x$ ; (b) airflow speed at the turbine duct  $V_x$  and pressure drop across the turbine  $\Delta p_t$ ; (c) turbine rotor angular velocity  $\Omega$  and its desired value  $\Omega_d$ ; (d) generator damping coefficient (control input)  $b_g$  and power extraction from the turbine  $P_t$ ; (e) turbine efficiency  $\eta_t$  and its maximum value  $\eta_{t,max}$ .

Figure 6 reveals that  $\bar{P}_t$  and  $\bar{\eta}_t$  increase as  $k_p$  increases. Beyond a  $k_p$  value of five,  $\bar{P}_t$  and  $\bar{\eta}_t$  reach a plateau, and no improvement of them can be observed. Conversely, as  $k_p$  increases,  $RMSE^*(\Omega)$  decreases drastically. Therefore, it appears that the optimal performance of the i-MET controller is reached as  $k_p$  increases. However, as seen in the Figure 5, when  $k_p = 10$ ,  $b_g$  tends to generate abnormal peaks as  $\Omega_d$  converges zero.

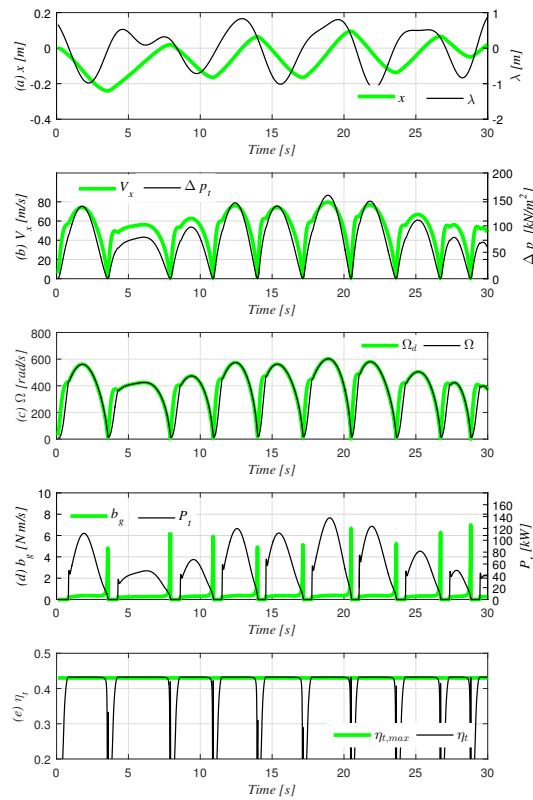


**Figure 5.** Simulation result of the first 30 s with the i-MET controller when  $k_p = 10$ : (a) wave  $\lambda$  and water column positions  $x$ ; (b) airflow speed at the turbine duct  $V_x$  and pressure drop across the turbine  $\Delta p_t$ ; (c) turbine rotor angular velocity  $\Omega$  and its desired value  $\Omega_d$ ; (d) generator damping coefficient (control input)  $b_g$  and power extraction from the turbine  $P_t$ ; (e) turbine efficiency  $\eta_t$  and its maximum value  $\eta_{t,max}$ .

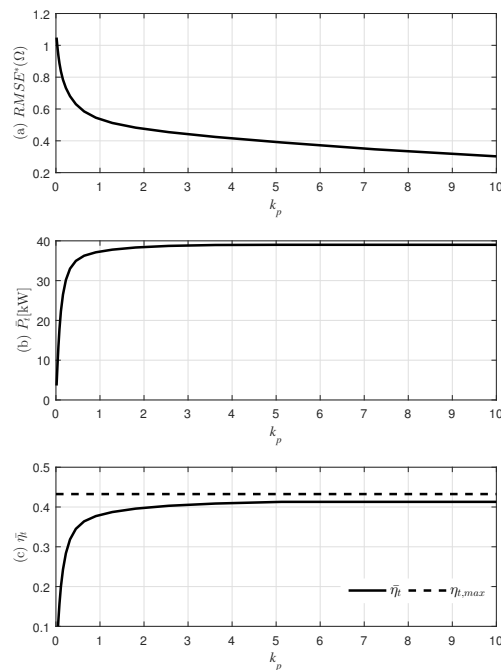


**Figure 6.** Results of the i-MET controller with various  $k_p$  under equivalent irregular wave conditions: (a) relative root mean squared error of  $\Omega$ ; (b) average power extraction from the turbine; (c) average turbine efficiency and its maximum value.

#### 4.2. Result of the CAV Controller

In order to evaluate the performance of the CAV controller, we set the  $\Omega_d$  as a constant to run the same simulation previously performed under the equivalent irregular waves, having a PM spectrum with  $T_p = 10$  s and  $H_s = 2$  m.

There are three factors that affect the CAV controller's performance:  $\Omega_d$ ,  $k_p$  and the inertia of the turbine and generator rotors  $J$ . Note that when  $b_g$  is constant, the variation of  $\Omega$  decreases as  $J$  increases. We first sought to observe the influence of  $k_p$  in the time domain. Figures 7 and 8 depict the simulation results of the OWC-turbine combined system with the CAV controller in the time domain where  $k_p = 0.05$  and 1, respectively, and  $\Omega_d = 250$  rad/s. Through comparing the two figures, it is apparent that a  $k_p$  value of one provides a faster convergence speed with a smaller error bound of  $\Omega$ .

When  $k_p$  is at one,  $\Omega$  converges to the  $\Omega_d$ . However, in both cases, we observe that the time interval of the maximum value of  $\eta_t$  is drastically reduced compared to that of the i-MET controller, as seen in Figure 5. Furthermore, as seen in Figures 7 and 8, the peaks of  $P_t$  and  $\eta_t$  are unmatched, causing the turbine's performance to have a negative effect on the total output.

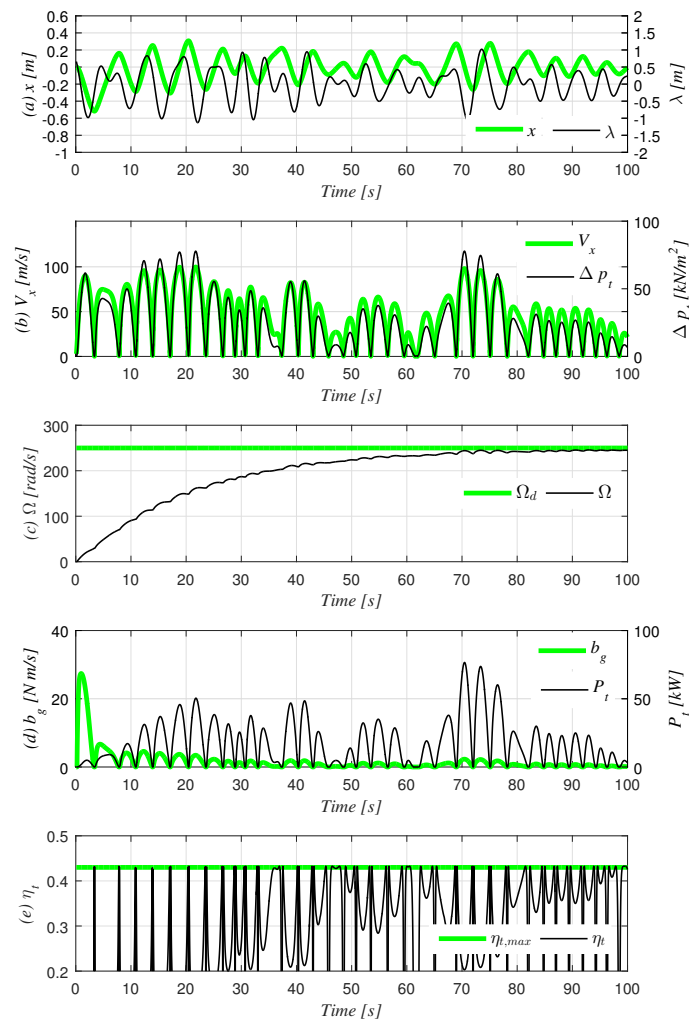


**Figure 7.** Simulation result of the first 100 s with the constant angular velocity (CAV) controller when  $\Omega_d = 250$  rad/s and  $k_p = 0.05$ : (a) wave  $\lambda$  and water column positions  $x$ ; (b) airflow speed at the turbine duct  $V_x$  and pressure drop across the turbine  $\Delta p_t$ ; (c) turbine rotor angular velocity  $\Omega$  and its desired value  $\Omega_d$ ; (d) generator damping coefficient (control input)  $b_g$  and power extraction from the turbine  $P_t$ ; (e) turbine efficiency  $\eta_t$  and its maximum value  $\eta_{t,max}$ .

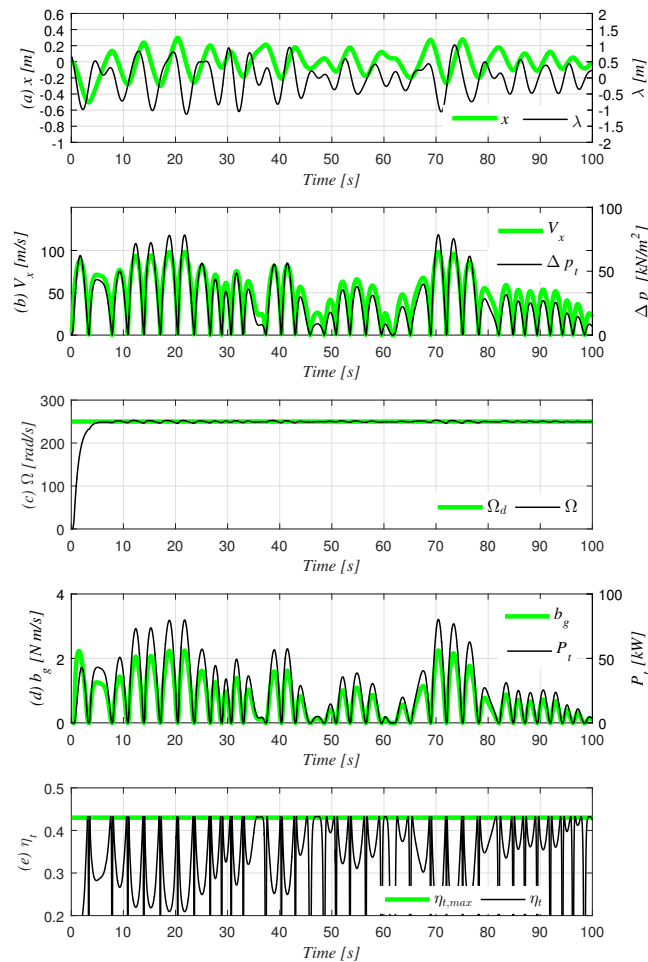


**Figure 8.** Simulation result of the first 100 s with the CAV controller when  $\Omega_d = 250$  rad/s and  $k_p = 1$ : (a) wave  $\lambda$  and water column positions  $x$ ; (b) airflow speed at the turbine duct  $V_x$  and pressure drop across the turbine  $\Delta p_t$ ; (c) turbine rotor angular velocity  $\Omega$  and its desired value  $\Omega_d$ ; (d) generator damping coefficient (control input)  $b_g$  and power extraction from the turbine  $P_t$ ; (e) turbine efficiency  $\eta_t$  and its maximum value  $\eta_{t,max}$ .

In order to more accurately observe the power extraction and the convergence of the angular velocity, we measured and compared their average values over a period of 5000 s. Figures 9–11 show the  $RMSE^*(\Omega)$ , average turbine power extraction  $\bar{P}_t$  and the average turbine efficiency  $\bar{\eta}_t$ , with respect to  $k_p$ , when  $\Omega_d$  is at 250, 400 and 550 rad/s.

As seen in Figures 9–11,  $RMSE^*(\Omega)$  converges to zero as  $k_p$  increases, as intended for control purposes. It should, however, be emphasized that the curve of  $RMSE^*(\Omega)$  with  $J = 1$  is lower than that with  $J = 5$  regardless of  $k_p$  in all cases. The CAV controller functions better when the inertia is smaller. This runs contrary to the results given when not using a controller. Hence, when not using a controller, a larger inertia results in smaller angular speed variation.

Unlike  $RMSE^*(\Omega)$ , which is the inverse of  $k_p$  independent of  $\Omega_d$ , the average power extraction  $\bar{P}_t$  and average turbine efficiency  $\bar{\eta}_t$  behave differently depending on the reference angular velocity  $\Omega_d$ .

The optimal average power extraction and average turbine efficiency is achieved when  $\Omega_d = 400$  rad/s (Figure 10). It should be noted that under these condition, when  $k_p$  increases,  $\bar{P}_t$ , and  $\bar{\eta}_t$  also increase. However, when  $\Omega_d = 550$  rad/s, the increase in  $k_p$  does not result in an overall increase in  $\bar{P}_t$  and  $\bar{\eta}_t$  (Figure 11).

To summarize, the convergence of the angular velocity is predominantly affected by the control gain  $k_p$ , while the average power extraction is influenced mainly by the reference angular velocity  $\Omega_d$ .

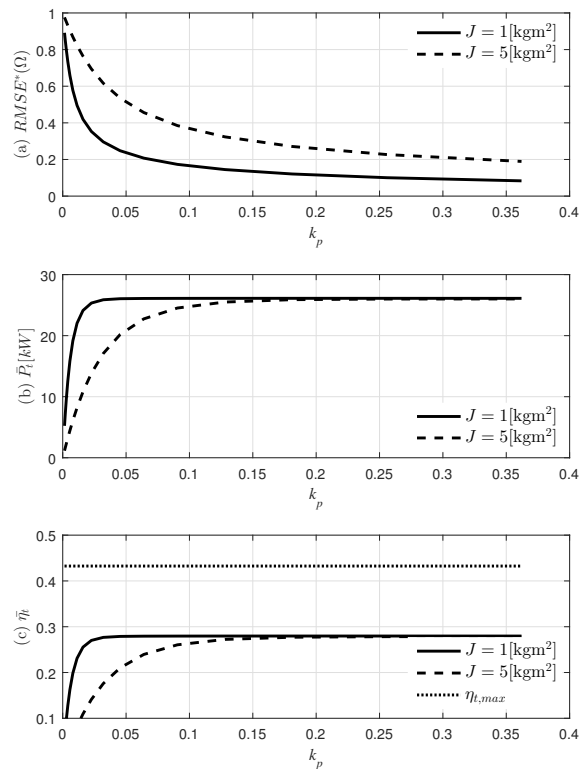


**Figure 9.** Results of the CAV controller with various  $k_p$  under an equivalent irregular wave condition when  $\Omega_d = 250 \text{ rad/s}$ : (a) relative root mean squared error of  $\Omega$ ; (b) average power extraction from the turbine; (c) average turbine efficiency and its maximum value.

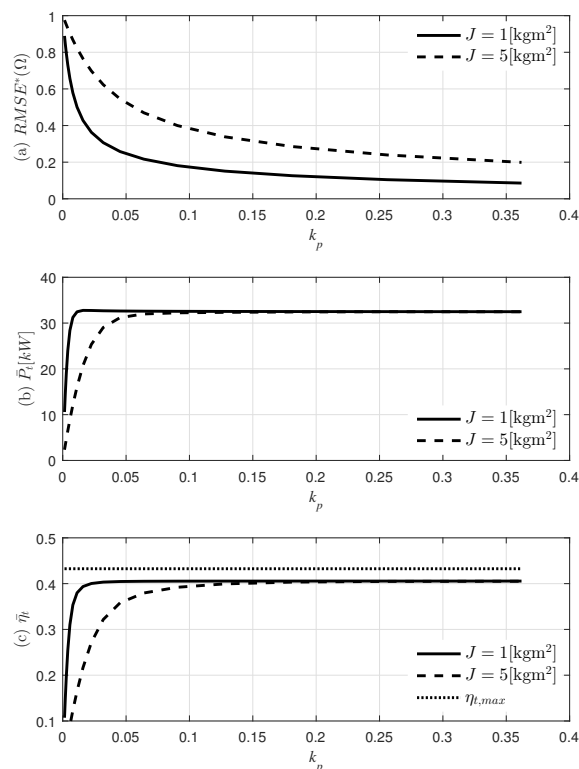


**Figure 10.** Results of the CAV controller with various  $k_p$  under an equivalent irregular wave condition when  $\Omega_d = 400 \text{ rad/s}$ : (a) relative root mean squared error of  $\Omega$ ; (b) average power extraction from the turbine; (c) average turbine efficiency and its maximum value.

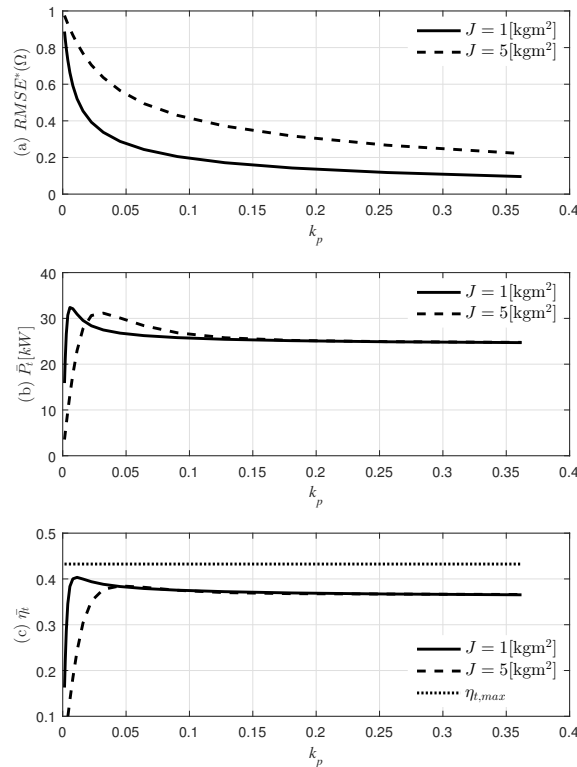


**Figure 11.** Results of the CAV controller with various  $k_p$  under an equivalent irregular wave condition when  $\Omega_d = 550 \text{ rad/s}$ : (a) relative root mean squared error of  $\Omega$ ; (b) average power extraction from the turbine; (c) average turbine efficiency and its maximum value.

### 5. Simulation Results under Irregular Conditions for Various Wave Period and Height

Here, we analyze differences between two previously-mentioned types of controllers in the set time domain. We show that increasing the instant efficiency of the turbine or maintaining a certain angular velocity will effect the converting efficiency of the chamber stage. Therefore, an analysis of how the overall system, including the chamber stage, influences the overall power output is needed.

In brief, our system consists of a chamber, turbine, DC electrical generator and terminal load attached to the generator. Due to the assumption that the only controllable parameter is the damping coefficient  $b_g$ , which is produced by the generator and decided by the load, from the electrical analysis point of view, the analysis with the simplest electrical component should precede, and constant linear damping is produced from the simplest electric component, the resistor. Additionally, the constant resistor  $R_e$  in (16) provides the constant damping coefficient  $b_g$ . Accordingly, we choose the results of constant damping  $b_g$  as the comparison results group for the controlled results. We set the standard as the maximum power extraction when  $b_g$  is at a constant.

Similar to the previous simulation, we measure the average power extraction  $\bar{P}_t$  with the same chamber, turbine and ocean state, when  $b_g$  is held constant. We obtained the maximum power extraction when  $b_g = 10^{-3} \sim 1$ , for the various  $H_s$  and  $T_p$ , by running a simulation for  $T_m = 5000 \text{ s}$ , when  $H_s$  was between  $0.4 \sim 5 \text{ m}$ , for every  $0.2 \text{ m}$ , and when  $T_p$  was between  $6 \sim 18 \text{ s}$ , for every  $1 \text{ s}$ . For the sake of convenience, we set the maximum power extraction with fixed  $b_g$  as  $\bar{P}_{t,max}$  and calculate accordingly.

$$\bar{P}_{t,max}(T_p, H_s) = \max_{b_g} \frac{1}{T_m} \int_0^{T_m} b_g \Omega^2 dt. \tag{31}$$

The damping coefficient at maximum power is defined as  $b_{g,max}$ . We also set the relative time average turbine efficiency as  $\bar{\eta}_t^* = \bar{\eta}_t / \eta_t(\phi_0)$ .

Figure 12 shows  $\bar{P}_{t,max}$ ,  $\bar{\eta}_t$  and  $b_{g,max}$  under irregular waves with a PM wave spectrum having various  $H_s$  and  $T_p$ . As seen in Figure 12c, in most areas except for those having a long wave period ( $T_p \geq 16$  s) and a low wave height ( $H_s \leq 0.6$  m),  $\eta_t^*$  is higher than 0.9. From this, it can be inferred that tracking the turbine efficiency is somewhat consistent with tracking the overall system performance.

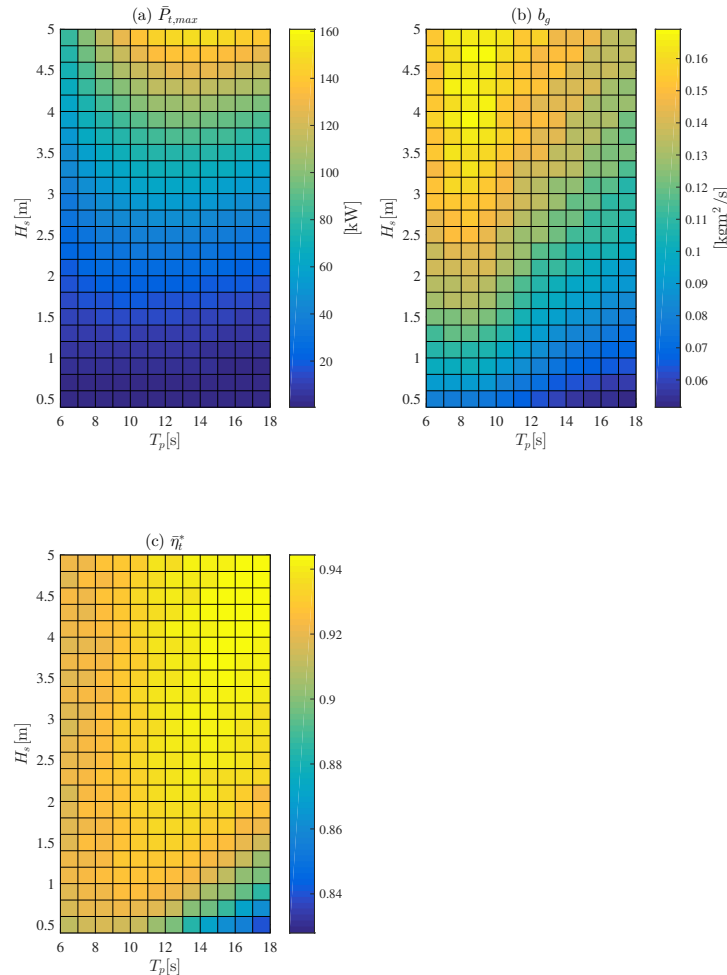


**Figure 12.** Time averaged results for maximum power extraction with  $b_g$  fixed in time under the Pierson–Moskowitz (PM) irregular wave model with various  $T_p$  and  $H_s$  for  $T_m = 5000$  s: (a) maximum power extraction from turbine; (b) generator damping coefficient; (c) relative turbine efficiency.

The results from the controllers will only deal with the power extraction with respect to  $\bar{P}_{t,max}$ , which is calculated as follows:

$$\bar{P}_t^* (T_p, H_s) = \frac{\bar{P}_t (T_p, H_s)}{\bar{P}_{t,max} (T_p, H_s)}. \tag{32}$$

### 5.1. i-MET Control Strategy

We determined  $\bar{P}_t^*$  and  $\bar{\eta}_t^*$  by performing  $T_m = 5000$  s simulations whilst using the i-MET controlled OWC-WEC system with  $k_p = 5$ . This was done in a PM wave environment with a peak period ( $T_p$ ) of 6~18 s and significant wave height ( $H_s$ ) of 0.4~5 m.

Figure 13 depicts the results when the i-MET controller is applied. Figure 13a shows the relative time average power extraction  $\bar{P}_t^*$ , and Figure 13b displays the relative turbine’s efficiency  $\bar{\eta}_t^*$ . In all areas,  $\bar{P}_t^*$  is at or above 0.94, with some areas exhibiting a performance above one.  $\bar{\eta}_t^*$  exhibits values greater than 0.95. We observed that  $\bar{P}_t^*$  is optimal in  $9 \leq T_p \leq 13$  and  $0.4 \leq H_s \leq 1.4$  and  $\bar{\eta}_t^*$  is optimal in  $12 \leq T_p$  and  $1 \leq H_s \leq 2$ . Thus, the correlation between the two seems minimal.

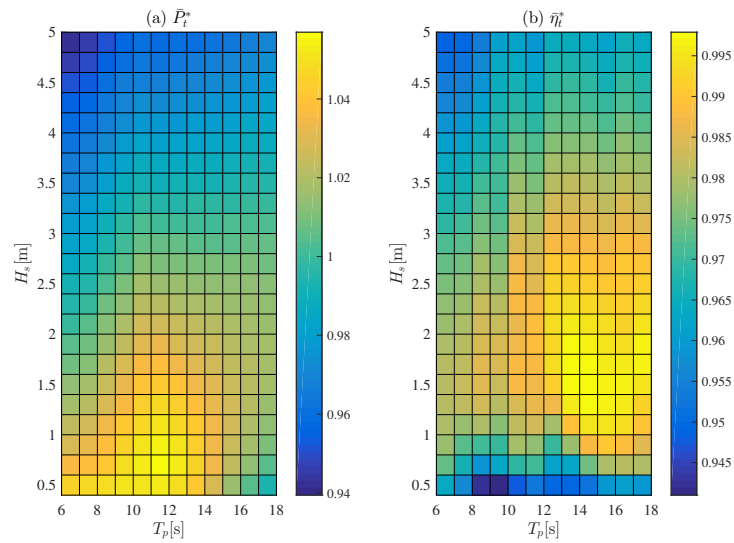


**Figure 13.** Time averaged results of the i-MET controller under the PM irregular wave model with various  $T_p$  and  $H_s$  for  $T_m = 5000$  s: (a) relative power extraction from turbine; (b) relative average turbine efficiency.

### 5.2. CAV Control Strategy

Under the equivalent conditions of previous simulations, we determined  $\bar{P}_t^*$  and  $\bar{\eta}_t^*$  whilst using the CAV-controlled OWC-WEC system with  $k_p = 0.2$ . Figures 14–16 depict results when using the CAV controller applied OWC-WEC system under various irregular wave states with a reference angular velocity of  $\Omega_d = 250, 400, 550$  rad/s, respectively. The overall analysis reveals that near optimum power extraction can be achieved through constant damping and a constant angular velocity. This, however, is dependent on an adequate reference angular velocity  $\Omega_d$  being maintained. Through data comparisons, we observed that an increase in wave height demands an increased reference angular velocity. In addition, since  $\bar{P}_t^*$  somewhat correlates to  $\bar{\eta}_t^*$ , we observe that  $\bar{\eta}_t^*$  plays an important role in the performance of the entire OWC-WEC system in this simulation.

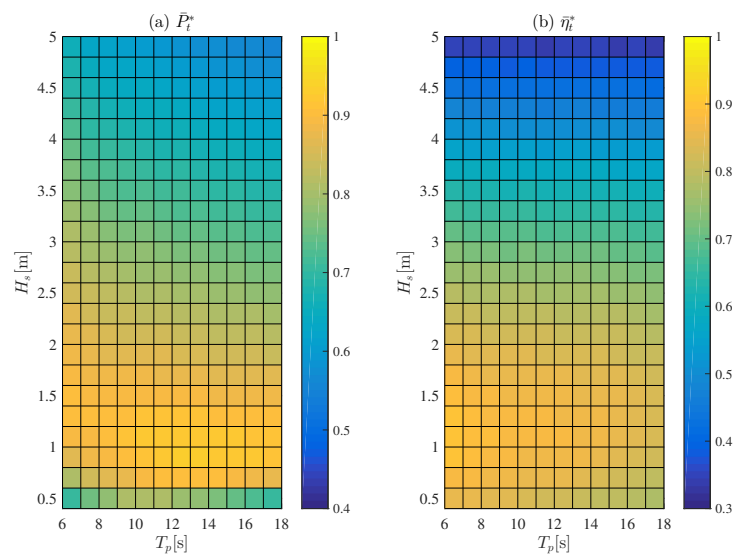


**Figure 14.** Time averaged results of the CAV controller under the PM irregular wave model with various  $T_p$  and  $H_s$  for  $T_m = 5000$  s when  $\Omega_d = 250$  rad/s: (a) relative power extraction from turbine; (b) relative average turbine efficiency.

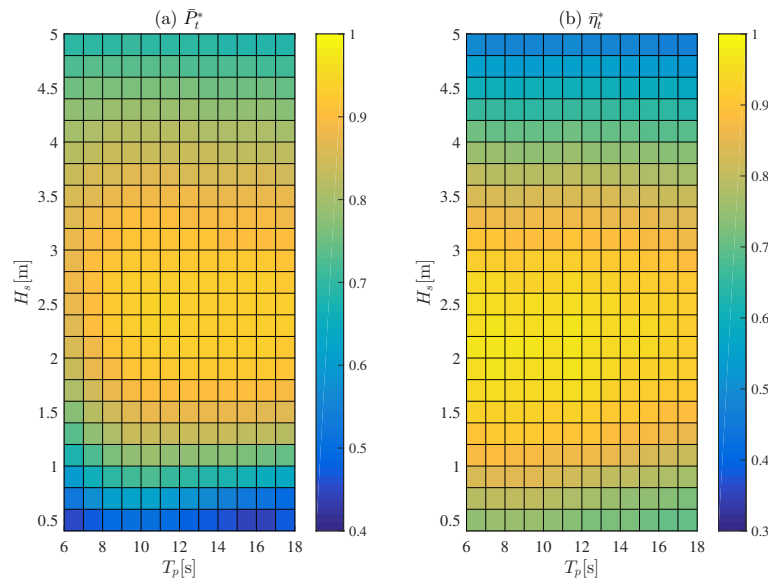


**Figure 15.** Time averaged results of the CAV controller under the PM irregular wave model with various  $T_p$  and  $H_s$  for  $T_m = 5000$  s when  $\Omega_d = 400$  rad/s: (a) relative power extraction from turbine; (b) relative average turbine efficiency.

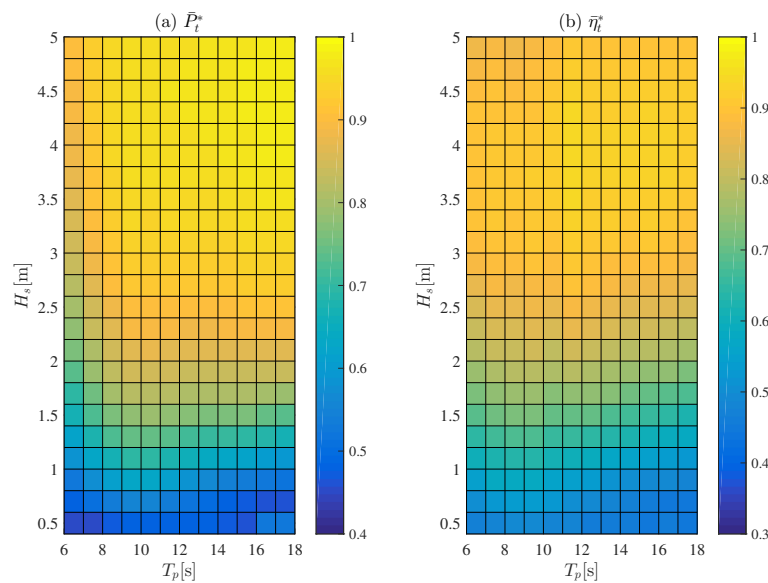


**Figure 16.** Time averaged results of the CAV controller under the PM irregular wave model with various  $T_p$  and  $H_s$  for  $T_m = 5000$  s when  $\Omega_d = 550$  rad/s: (a) relative power extraction from turbine; (b) relative average turbine efficiency.

### 6. Conclusions

The system’s overall efficiency is heavily influenced by the efficiency of each sub-unit. This is due to the OWC-WEC attaching to the total system in the order of chamber-turbine-generator. The chamber and turbine, which are the first sub-units, are directly affected by the physical damping term that is produced from the generator and have a mutual influence on each other. Therefore, it is difficult to strategize a real-time method to maximize the entire system efficiency. Otherwise, analysis of the time domain is subject to the Newtonian mechanics, and it does not require the constant angular speed of the turbine that was assumed in the frequency domain analysis, since the angular acceleration level of the turbine can be addressed in the Newtonian mechanics.

Thus, we have discussed the real-time control strategy under the assumption that it is related to an ideal electric DC generator, of which we can only control its terminal load. We designed the controller with two objectives in mind: (1) maximizing the turbine's instant efficiency (i-MET); and (2) regulating the turbine's spin speed (CAV). We then demonstrated the effectiveness of the controller by applying it to an OWC-turbine combined WEC system under an irregular wave environment, running a simulation in the time domain and comparing it to the maximum when the terminal load is constant with  $b_g$  between  $10^{-3}$  and one.

The i-MET controller, which tracks the turbine's maximum efficiency, requires the function of the input and torque coefficients, as well as real-time measuring of the turbine's angular velocity and air flow speed. This simulation assumes that the turbine's characteristics are quasi-static. As seen in the results of Section 4, the turbine's instant efficiency was at its maximum within its functional intervals. Since tracking the turbine's maximum efficiency does not guarantee the optimal operation of the WEC-system as a whole, we compared the power extraction obtained by the controllers with the maximum power extraction that has no control under a constant damping coefficient with irregular waves that have varying wave heights and periods. Figure 13, which depicts the relative power extractions and relative efficiencies, reveals that the system maintains a relative power extraction over 0.94 for most wave states. This system also manages to achieve relative power extractions greater than one in certain states and also provides a relative turbine efficiency over 0.94 in most areas. In addition, it can be inferred that there is no correlation between relative power extractions and relative efficiencies with the i-MET controller. As seen in Figures 4 and 5, the angular velocity of the rotor fluctuates with the i-MET controller that yields a very poor quality of electricity. However, the value of this controller rests on the fact that we can measure the maximum power extraction without knowledge of the ideal damping load in a chamber-turbine-generator combined system. The i-MET controller can be regarded as a type of MPPT (maximum power point tracking) controller in the aspect of a controller for maximum output. While the general MPPT algorithm decides the load condition by comparison between the averaged current and past performances [52], the i-MET controller decides the load condition by comparison between the current and reference states. Hence, the MPPT is suitable for applications such as photo-voltaic [53] and wind power generators with consistent sunlight and wind speed [54], respectively. However, it is hard to design the real-time MPPT controller for the wave energy converter due to the strong irregularity. On the other hand, the i-MET controller has the turbine efficiency curves as the reference, which have the optimal point. Hence, it is possible to build a real-time control algorithm based on the Lyapunov method. The Lyapunov method provides the real-time control law when the system is dynamic and the reference signal with the optimal point exists.

The CAV controller uses the same control algorithm in order to track the set angular velocity; however, the reference angular velocity is constant. Therefore, the CAV controller shares the same states (air flow speed and turbine angular velocity) and assumptions as needed for the implementation of the i-MET controller. When the CAV controller is applied, the angular velocity converges to the desired value as the control gain increases. Simulations reveal that the overall power extraction is influenced mainly by the reference angular velocity, which is somewhat proportional to the wave height. Compared to the i-MET controller, the CAV controller needs to adjust the reference angular velocity depending on the wave state. Nonetheless, the CAV controller seems to be the more realistic control strategy when considering the optimal performance of the inverter, since it employs a generator that rotates at a constant speed providing a constant voltage. This allows a more realistic performance analysis of OWC-WEC.

In order to implement the i-MET and CAV controllers practically, more realistic modeling with the physical limitations of the hydrodynamics of the chamber and the aerodynamics of the turbine should be considered. Furthermore, unlike the ideal DC generator, electric machine modeling should have the nonlinear torque-rpm curve with an actual efficiency curve. In addition, the inverter modeling that produces the control input for the terminal load should be developed under the consideration of substantial hardware specifications. Details on that will be covered in future studies.

**Acknowledgments:** The presented work was supported by ENGINE Inc.

**Author Contributions:** Seung Kwan Song conceived and designed the simulations; Seung Kwan Song performed the simulations; Seung Kwan Song and Jin Bae Park analyzed the data; Seung Kwan Song wrote the paper.

**Conflicts of Interest:** The authors declare no conflict of interest.

## Abbreviations

The following abbreviations are used in this manuscript:

$a_c, a_t$	Cross-sectional area of the chamber and turbine duct
$b_g$	Generator damping coefficient
$b_t$	Blade span
$f_r$	Radiation memory function
$h_0$	Chamber tube draft
$k_h$	Hydrostatic stiffness
$k_p$	Proportional control gain
$l_t$	Chord length of the turbine rotor blade
$n_t$	Number of turbine rotor blades
$\Delta p_c$	Pressure difference between the chamber and atmosphere
$\Delta p_t$	Pressure drop across the turbine
$\Delta \omega_t$	Small wave angular frequency interval
$r_t$	Turbine rotor mean radius
$t$	Time
$x$	Vertical position of the inner water level
$z$	State vector for $F_r$
$A, B, C$	State-space matrices for the approximation of $F_r$
$C_a, C_t$	Input and torque coefficients
$E_g$	Induced generator voltage
$F_e$	Excitation force
$F_r$	Convolution part of the radiation force
$H_s$	Significant wave height
$I_a$	Circuit current
$J$	Inertia of the turbine and generator rotors
$K_g$	Generator torque proportionality constant
$M$	Mass of trapped water in the chamber
$N$	Arbitrary number
$P_g, P_t$	Power extraction from the generator and turbine
$P_{pne}$	Pneumatic incident power
$Q$	Flow rate
$R_a, R_e$	Internal and external loads
$S_{PM}$	Pierson–Moskowitz’s wave energy spectrum
$T_p$	Wave peak period
$V$	Lyapunov candidate function
$V_x$	Airflow speed at the turbine duct
$\gamma, \epsilon$	Positive constants
$\eta_t$	Turbine efficiency
$\theta_n$	Initial phase of the wave component of order $n$
$\lambda(t)$	Wave elevation
$\lambda_n$	Amplitude of the wave component of order $n$
$\mu(\infty)$	Added mass at infinite frequency

$\rho_a, \rho_w$	Air and seawater density
$\tau_g, \tau_t$	Induced torques from the generator and turbine
$\phi, \phi_o$	Flow coefficient and optimal value at the maximum turbine efficiency
$\omega$	Wave angular frequency
$\omega_n$	$n'$ -th order wave angular frequency
$\omega_l$	Lowest wave angular frequency
$\Omega$	Angular velocity of the turbine rotor
$\Omega_d$	Desired angular velocity of the turbine rotor
*	Relative value with respect to the ideal case or the maximum value
~	Error value
-	Average value

## References

1. Mørk, G.; Barstow, S.; Kabuth, A.; Pontes, M.T. Assessing the global wave energy potential. In Proceedings of the 29th International Conference on Ocean, Offshore and Arctic Engineering, Shanghai, China, 6–11 June 2010; Volume 20473.
2. Arena, F.; Laface, V.; Malara, G.; Romolo, A.; Viviano, A.; Fiamma, V.; Sannino, G.; Carillo, A. Wave climate analysis for the design of wave energy harvesters in the Mediterranean Sea. *Renew. Energy* **2015**, *77*, 125–141.
3. Falcão, A.F.O.; Henriques, J.C.C. Oscillating-water-column wave energy converters and air turbines: A review. *Renew. Energy* **2016**, *85*, 1391–1424.
4. Lindroth, S.; Leijon, M. Offshore wave power measurements—A review. *Renew. Sustain. Energy Rev.* **2011**, *15*, 4274–4285.
5. Viviano, A.; Naty, S.; Foti, E.; Bruce, T.; Allsop, W.; Vicinanza, D. Large-scale experiments on the behaviour of a generalised Oscillating Water Column under random waves. *Renew. Energy* **2016**, *99*, 875–887.
6. Falcão, A.F.O.; Henriques, J.C.C.; Gato, L.M.C.; Gomes, R.P.F. Air turbine choice and optimization for floating oscillating-water-column wave energy converter. *Ocean Eng.* **2014**, *75*, 148–156.
7. Gomes, R.P.F.; Henriques, J.C.C.; Gato, L.M.C.; Falcão, A.F.O. Hydrodynamic optimization of an axisymmetric floating oscillating water column for wave energy conversion. *Renew. Energy* **2012**, *44*, 328–339.
8. Falcão, A.F.O.; Henriques, J.C.C.; Cândido, J.J. Dynamics and optimization of the OWC spar buoy wave energy converter. *Renew. Energy* **2012**, *48*, 369–381.
9. Falcão, A.F.O. Stochastic modelling in wave power-equipment optimization: Maximum energy production versus maximum profit. *Ocean Eng.* **2004**, *31*, 1407–1421.
10. Evans, D.V. Power from water waves. *Annu. Rev. Fluid Mech.* **1981**, *13*, 157–187.
11. Falnes, J. Optimum control of oscillation of wave-energy converters. *Int. J. Offshore Polar Eng.* **2002**, *12*, 1–12.
12. Falnes, J. *Ocean Waves and Oscillating Systems: Linear Interactions Including Wave-Energy Extraction*; Cambridge University Press: Cambridge, UK, 2002.
13. Genest, R.; Bonnefoy, F.; Clément, A.H.; Babarit, A. Effect of non-ideal power take-off on the energy absorption of a reactively controlled one degree of freedom wave energy converter. *Appl. Ocean Res.* **2014**, *48*, 236–243.
14. Tedeschi, E.; Carraro, M.; Molinas, M.; Mattavelli, P. Effect of control strategies and power take-off efficiency on the power capture from sea waves. *IEEE Trans. Energy Convers.* **2011**, *26*, 1088–1098.
15. Falnes, J.; Budal, K. Wave-power conversion by point absorbers. *Nor. Marit. Res.* **1978**, *6*, 2–11.
16. Falnes, J. Wave-energy conversion through relative motion between two single-mode oscillating bodies. *J. Offshore Mech. Arct. Eng.* **1999**, *121*, 32–38.
17. Falcão, A.F.O.; Justino, P.A.P.; Henriques, J.C.C.; André, J.M.C.S. Reactive versus latching phase control of a two-body heaving wave energy converter. In Proceedings of the 2009 European on European Control Conference, Budapest, Hungary, 23–26 August 2009; pp. 3731–3736.
18. Masuda, Y. Wave-Activated Generator. In Proceedings of the International Colloquium on the Expositions of the Oceans, Bordeaux, France, 3–5 March 1971.
19. Masuda, Y. An experience of wave power generator through tests and improvement. In *Hydrodynamics of Ocean Wave-Energy Utilization*; Springer: Berlin, Germany, 1986; pp. 445–452.

20. Masuda, Y.; McCormick, M.E. Experiences in pneumatic wave energy conversion in Japan. In Proceedings of the Utilization of Ocean Waves-Wave to Energy Conversion, ASCE, La Jolla, CA, USA, 16–17 June 1986; pp. 1–33.
21. Falcão, A.F.O. The shoreline OWC wave power plant at the Azores. In Proceedings of the 4th European Wave Energy Conference, Aalborg, Denmark, 4–6 December 2000; pp. 42–48.
22. Heath, T.; Whittaker, T.J.T.; Boake, C.B. The design, construction and operation of the LIMPET wave energy converter (Islay, Scotland). In Proceedings of the 4th European Wave Energy Conference, Aalborg, Denmark, 4–6 December 2000; pp. 49–55.
23. Zhang, D.; Li, W.; Lin, Y. Wave energy in China: Current status and perspectives. *Renew. Energy* **2009**, *34*, 2089–2092.
24. McCormick, M.E. A theoretical analysis of a self-propelled backward-bent duct wave energy conversion system. *J. Energy Resour. Technol.* **1991**, *113*, 94–100.
25. Hong, D.C.; Hong, S.Y.; Hong, S.W. Numerical study on the reverse drift force of floating BBDB wave energy absorbers. *Ocean Eng.* **2004**, *31*, 1257–1294.
26. Washio, Y.; Osawa, H.; Nagata, Y.; Fujii, F.; Furuyama, H.; Fujita, T. The offshore floating type wave power device “Mighty Whale”: Open sea tests. In Proceedings of the Tenth International Offshore and Polar Engineering Conference, Seattle, WA, USA, 28 May–2 June 2000; pp. 373–380.
27. Setoguchi, T.; Santhakumar, S.; Maeda, H.; Takao, M.; Kaneko, K. A review of impulse turbines for wave energy conversion. *Renew. Energy* **2001**, *23*, 261–292.
28. Maeda, H.; Santhakumar, S.; Setoguchi, T.; Takao, M.; Kinoue, Y.; Kaneko, K. Performance of an impulse turbine with fixed guide vanes for wave power conversion. *Renew. Energy* **1999**, *17*, 533–547.
29. Raghunathan, S. The Wells air turbine for wave energy conversion. *Prog. Aeros. Sci.* **1995**, *31*, 335–386.
30. Gato, L.M.C.; Falcão, A.F.O. Aerodynamics of the wells turbine: Control by swinging rotor-blades. *Int. J. Mech. Sci.* **1989**, *31*, 425–434.
31. Gato, L.M.C.; Eça, L.R.C.; Falcão, A.F.O. Performance of the Wells turbine with variable pitch rotor blades. *J. Energy Resour. Technol.* **1991**, *113*, 141–146.
32. Perdigao, J.; Sarmento, A. Overall-efficiency optimisation in OWC devices. *Appl. Ocean Res.* **2003**, *25*, 157–166.
33. Jefferys, R.; Whittaker, T. Latching control of an oscillating water column device with air compressibility. In *Hydrodynamics of Ocean Wave-Energy Utilization*; Springer: Berlin, Germany, 1986; pp. 281–291.
34. Hoskin, R.E.; Count, B.M.; Nichols, N.K.; Nicol, D.A.C. Phase control for the oscillating water column. In *Hydrodynamics of Ocean Wave-Energy Utilization*; Springer: Berlin, Germany, 1986; pp. 257–268.
35. Falcão, A.F.O.; Rodrigues, R.J.A. Stochastic modelling of OWC wave power plant performance. *Appl. Ocean Res.* **2002**, *24*, 59–71.
36. Falcão, A.F.O. Control of an oscillating-water-column wave power plant for maximum energy production. *Appl. Ocean Res.* **2002**, *24*, 73–82.
37. Ceballos, S.; Rea, J.; Lopez, I.; Pou, J.; Robles, E.; O’Sullivan, D.L. Efficiency optimization in low inertia wells turbine-oscillating water column devices. *IEEE Trans. Energy Convers.* **2013**, *28*, 553–564.
38. Alberdi, M.; Amundarain, M.; Garrido, A.J.; Garrido, I.; Casquero, O.; De la Sen, M. Complementary control of oscillating water column-based wave energy conversion plants to improve the instantaneous power output. *IEEE Trans. Energy Convers.* **2011**, *26*, 1021–1032.
39. Amundarain, M.; Alberdi, M.; Garrido, A.J.; Garrido, I. Modeling and simulation of wave energy generation plants: Output power control. *IEEE Trans. Ind. Electron.* **2011**, *58*, 105–117.
40. Khalil, H.K.; Grizzle, J.W. *Nonlinear Systems*; Prentice Hall: Upper Saddle River, NJ, USA, 1996; Volume 3.
41. Weinstein, M.I. Lyapunov stability of ground states of nonlinear dispersive evolution equations. *Commun. Pure Appl. Math.* **1986**, *39*, 51–67.
42. Goldhirsch, I.; Sulem, P.L.; Orszag, S.A. Stability and Lyapunov stability of dynamical systems: A differential approach and a numerical method. *Phys. D Nonlinear Phenom.* **1987**, *27*, 311–337.
43. Garrido, A.J.; Garrido, I.; Amundarain, M.; Alberdi, M.; De la Sen, M. Sliding-mode control of wave power generation plants. *IEEE Trans. Ind. Appl.* **2012**, *48*, 2372–2381.
44. Wahyudie, A.; Jama, M.A.; Saeed, O.; Noura, H.; Assi, A.; Harib, K. Robust and low computational cost controller for improving captured power in heaving wave energy converters. *Renew. Energy* **2015**, *82*, 114–124.

45. Kim, S.H.; Ryu, W.J.; Shin, S.H.; Hong, K.Y.; Kim, Y.D.; Kim, G.W. Application of the Orifice as a Turbine Substitute of OWC Wave Energy Converter. Available online: <http://www.dbpia.co.kr/Article/NODE02040148> (accessed on 28 September 2016).
46. El Hawary, M.E. *Principles of Electric Machines with Power Electronic Applications*; Wiley-IEEE Press: Hoboken, NJ, USA, 1986.
47. Falcão, A.F.O.; Justino, P.A.P. OWC wave energy devices with air flow control. *Ocean Eng.* **1999**, *26*, 1275–1295.
48. Butcher, J.C. *The Numerical Analysis of Ordinary Differential Equations: Runge-Kutta and General Linear Methods*; Wiley-Interscience: Hoboken, NJ, USA, 1987.
49. ANSYS, A. *User Manual v. 13.0*; Century Dynamics Ltd.: Horsham, UK, 2010.
50. Bosma, B.; Zhang, Z.; Brekken, T.K.A.; Özkan-Haller, H.T.; McNatt, C.; Yim, S.C. Wave energy converter modeling in the frequency domain: A design guide. In Proceedings of the IEEE on Energy Conversion Congress and Exposition (ECCE), Raleigh, NC, USA, 15–20 September 2012; pp. 2099–2106.
51. Gōda, Y. *Random Seas and Design of Maritime Structures*; World Scientific: Singapore, 2010.
52. Khaligh, A.; Onar, O.C. *Energy Harvesting: Solar, Wind, and Ocean Energy Conversion Systems*; CRC Press: Boca Raton, FL, USA, 2009.
53. Xiao, W.; Dunford, W.G. A modified adaptive hill climbing MPPT method for photovoltaic power systems. In Proceedings of the IEEE Power Electronics Specialists Conference, Aachen, Germany, 20–26 June 2004; Volume 3, pp. 1957–1963.
54. Kazmi, S.M.R.; Goto, H.; Guo, H.J.; Ichinokura, O. A novel algorithm for fast and efficient speed-sensorless maximum power point tracking in wind energy conversion systems. *IEEE Trans. Ind. Electron.* **2011**, *58*, 29–36.



© 2016 by the authors; licensee MDPI, Basel, Switzerland. This article is an open access article distributed under the terms and conditions of the Creative Commons Attribution (CC-BY) license (<http://creativecommons.org/licenses/by/4.0/>).